Hot carrier extraction in CH3NH3PbI3 unveiled by pump-push-probe spectroscopy

Lim, Swee Sien; Giovanni, David; Zhang, Qiannan; Solanki, Ankur; Jamaludin, Nur Fadilah; Lim, Jia Wei Melvin; Mathews, Nripan; Mhaisalkar, Subodh; Pshenichnikov, Maxim S.; Sum, Tze Chien

Published in:
Science Advances

DOI:
10.1126/sciadv.aax3620

Publication date:
2019

OPTICS

Hot carrier extraction in $CH_3NH_3PbI_3$ unveiled by pump-push-probe spectroscopy

Swee Sien Lim[1]*, David Giovanni[1]*, Qiannan Zhang[1], Ankur Solanki[1], Nur Fadilah Jamaludin[2,3,4], Jia Wei Melvin Lim[1,2], Nripan Mathews[3,4], Subodh Mhaisalkar[3,4], Maxim S. Pshenichnikov[1,5†], Tze Chien Sum[1†]

Halide perovskites are promising materials for development in hot carrier (HC) solar cells, where the excess energy of above-bandgap photons is harvested before being wasted as heat to enhance device efficiency. Presently, HC separation and transfer processes at higher-energy states remain poorly understood. Here, we investigate the excited state dynamics in $CH_3NH_3PbI_3$ using pump-push-probe spectroscopy. It has its intrinsic advantages for studying these dynamics over conventional transient spectroscopy, albeit complementary to one another. By exploiting the broad excited-state absorption characteristics, our findings reveal the transfer of HCs from these higher-energy states into bathophenanthroline (bphen), an energy selective organic acceptor far above perovskite's band edges. Complete HC extraction is realized only after overcoming the interfacial barrier formed at the heterojunction, estimated to be between 1.01 and 1.08 eV above bphen's lowest unoccupied molecular orbital level. The insights gained here are essential for the development of a new class of optoelectronics.

INTRODUCTION

Organic-inorganic halide perovskites, e.g., methylammonium lead iodide ($CH_3NH_3PbI_3$, or MAPI), have emerged as low-cost, high-performing materials for solar cells exceeding 20% (*1*), along with light-emitting (*2*, *3*) and lasing devices (*4*, *5*). The performance of perovskite solar cells has seen tremendous improvements within a few years, primarily driven by optimization of growth techniques, careful interfacial engineering, and process controls. In addition, perovskite's intrinsic optical properties, such as high optical absorption coefficients, long carrier diffusion lengths, and low trap state densities, coupled with its defect tolerance, make it an exceptionally good photoactive material for solar cells. However, improvements to the power conversion efficiency (PCE), especially in the past 2 years, have slowed down substantially. The state-of-the-art perovskite cells (~23%) are still far from the Shockley-Queisser limits of about 31% for a bandgap of 1.6 eV (*6*). As it becomes increasingly difficult to improve PCE in homojunction cells, more advanced photovoltaic concepts should be explored.

In homojunction cells, relaxation of hot carriers (HCs) is a major cause of energy loss. HCs are produced when photons with energies larger than the semiconductor's bandgap create carriers with excess kinetic energies. Following photoexcitation, carrier thermalization occurs owing to ultrafast scattering processes, e.g., carrier-carrier or carrier–optical phonon scattering (*7*, *8*). The ensuing broadening of the carrier population results in a quasi-equilibrium carrier temperature higher than the lattice. Carrier cooling subsequently occurs because of carrier-phonon or carrier-impurity scattering, resulting in a thermal equilibrium of the carriers with the lattice within subpicosecond time scales (*7*). Much higher solar cell efficiencies are possible if the excess energy is harvested before being wasted as heat. HC extraction is therefore a highly desirable approach to exceed the fundamental Shockley-Queisser limit and achieve higher efficiencies (*9*). In unconcentrated sunlight, given a 100% efficient extraction, an HC solar cell with a semiconductor having a bandgap of 1.6 eV (e.g., MAPI) can theoretically achieve PCE >40% in the presence of dominant Auger recombination and up to 66% (*10*) when Auger losses are negligible. Nonetheless, the realization of HC extraction is extremely challenging in conventional semiconductors, given the competing and more energetically favorable ultrafast relaxation process. One key criterion for favorable HC extraction is to slow HC relaxation to the time scale of energy extraction.

Recently, halide perovskites are found to exhibit slow HC cooling properties (*11*, *12*) favorable for application as HC absorbers. This phenomenon has been attributed to various origins: (i) hot phonon bottleneck (*13*, *14*), (ii) band-filling effects (*15*), (iii) large polaron (*16*), and (iv) Auger heating (*14*) at higher carrier densities. At present, the HC cooling lifetimes are still a subject of debate due to aforementioned slowing mechanisms. For (ii), formamidinium tin triiodide ($FASnI_3$) photoluminescence from hot carriers was reported (*15*) to be unexpectedly long (a few nanoseconds), which was assigned to state filling of band-edge states. For (iii), Zhu *et al.* (*16*) proposed that the polar organic molecules in bulk perovskites provide charge screening (i.e., large polaron formation) and hence prolong the HC lifetimes up to >150 ps at a low excitation density of ~7×10^{16} cm^{-3}. This observation, however, contrasts with other reports, where HC cooling is reported to be much faster, at ~0.1 ps at carrier densities <5×10^{17} cm^{-3} (*14*, *17*, *18*) and ~30 ps at excitation densities >5×10^{18} cm^{-3} (*13*). Hence, the interplay of the lattice effects and electronic properties remains an open question. Against this backdrop, several exciting reports that aptly highlighted the potential of perovskites for HC solar cells emerged: Li *et al.* (*19*) slowed down the HC cooling by

[1]Division of Physics and Applied Physics, School of Physical and Mathematical Sciences, Nanyang Technological University, 21 Nanyang Link, Singapore 637371, Singapore. [2]Energy Research Institute @NTU (ERI@N), Interdisciplinary Graduate School, Nanyang Technological University, Singapore, Singapore. [3]Energy Research Institute @NTU (ERI@N), Research Techno Plaza, X-Frontier Block, Level 5, 50 Nanyang Drive, Singapore 637553, Singapore. [4]School of Materials Science and Engineering, Nanyang Technological University, Nanyang Avenue, Singapore 639798, Singapore. [5]Zernike Institute for Advanced Materials, University of Groningen, Groningen, Netherlands.
*These authors contributed equally to this work.
†Corresponding author. Email: tzechien@ntu.edu.sg (T.C.S.); m.s.pchenitchnikov@rug.nl (M.S.P.)

almost two orders of magnitude using quantum confinement and demonstrated HC extraction from $MAPbBr_3$ nanocrystals, while Guo *et al.* (*20*) demonstrated long HC transport lengths of ~600 nm in MAPI thin films. Most recently, leveraging on the slow HC cooling properties, Li *et al.* (*21*) further realized low threshold and multiple exciton generation in $FAPbI_3$ nanocrystals. A clear understanding of the intrinsic photophysics, especially the dynamics of the higher-energy states in perovskites, holds the key to the design and optimization of new perovskites for HC photovoltaics.

One powerful time-resolved optical technique to directly probe such ultrafast transient states is pump-push-probe (PPP) spectroscopy (*22*, *23*). This technique is most commonly applied in the highly excitonic organic photoactive systems, where evidence of charge generation from the higher excited states was uncovered (*23*–*26*). Unlike conventional pump-probe spectroscopy, PPP could circumvent complexities arising from multiband excitation and density-dependent multiparticle effects that could obfuscate interpretation. A better understanding of the HC relaxation dynamics and its potential for charge transfer is crucial in designing appropriate acceptor layers to realize functional HC perovskite solar cells. In this work, we probe the HC extraction from MAPI thin films by observing the cooling dynamics of the photoexcited carriers. This is realized by contacting a non-injecting charge acceptor layer with MAPI and using a push pulse with sufficient photon energy to overcome the interfacial band offsets for HC transfer to the acceptor layer. Monitoring the presence or absence of ultrafast cooling provides a wealth of information on whether HC transfer has occurred. Our findings shed new light on the HC dynamics in the higher-energy states that could pave the way to conceptualizing new device architectures for efficient perovskite solar cells and optoelectronic devices.

RESULTS

Carrier relaxation probed by PPP spectroscopy

Figure 1A shows the typical transient absorption (TA) spectra of MAPI at different pump-probe delays. There are three dominant features observed: two photobleaching peaks (PB1 and PB2, $\Delta T/T > 0$) and a broad photoinduced absorption (PIA; $\Delta T/T < 0$) band. It is well

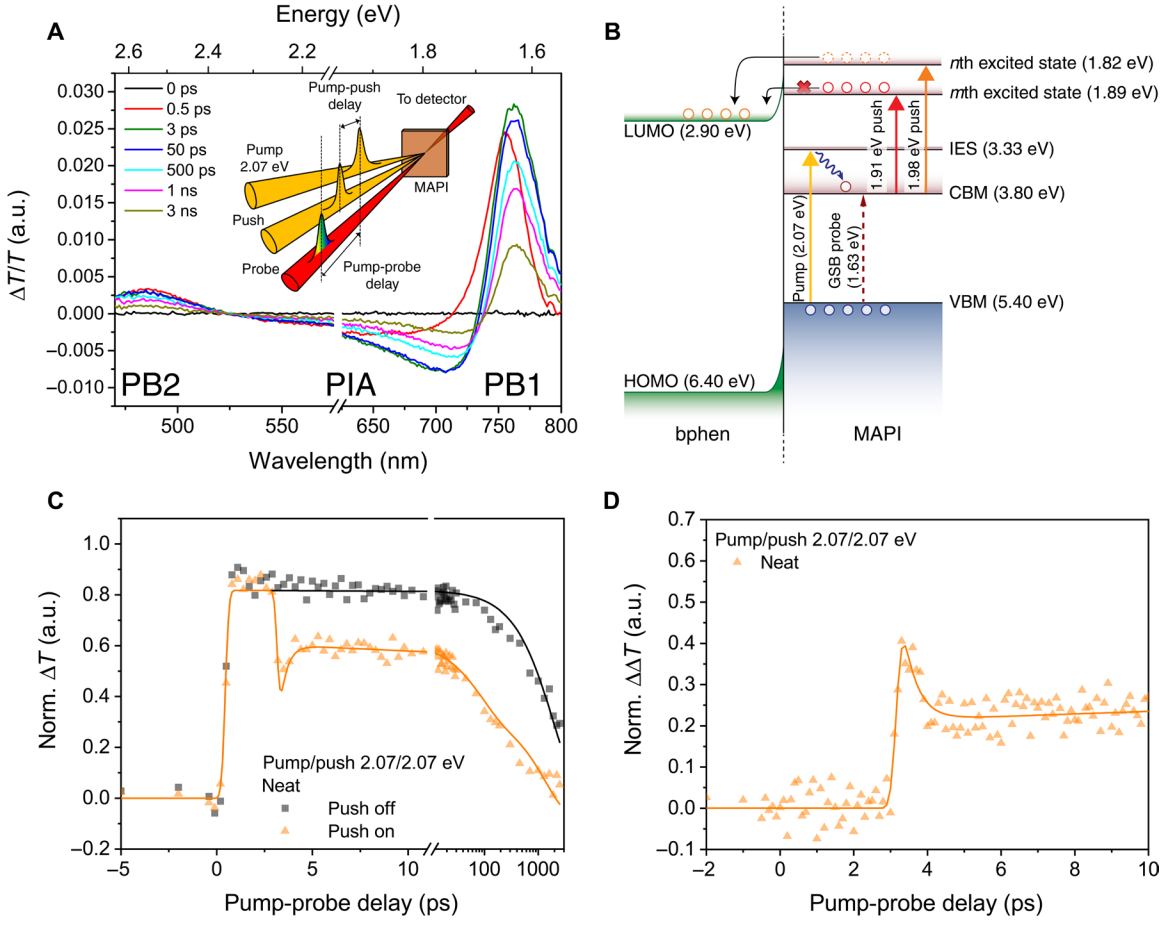

Fig. 1. PPP spectroscopy on MAPI. (**A**) Representative pump-probe TA spectra of MAPI at different pump-probe delays using a 2.07-eV (600 nm) pump. Inset: A schematic of our three-pulse PPP experiment. a.u., arbitrary units. (**B**) The influence of push pulses of varying photon energies on the thermalized carriers. Injection of HCs to bphen occurs if the push could overcome the band offset and the interfacial barrier of bphen. IES, initial excited state; HOMO, highest occupied molecular orbital; LUMO, lowest unoccupied molecular orbital. (**C**) PPP ΔT transients of MAPI without bphen (neat film, black and orange solid symbols for push off and on, respectively) probed at PB1 [the 1.63-eV ground-state bleaching (GSB) and stimulated emission (SE)]. The 2.07 eV push pulse (15 μJ cm^{-2}) arrives 3 ps after the 2.07-eV pump (5 μJ cm^{-2}). The solid lines are multiexponential fits of the pump-probe and PPP kinetics. (**D**) The corresponding $\Delta\Delta T$ push-induced signal and fit transients are obtained by taking the difference of the ΔT transients [push off–push on in (C)]. The time window is cropped for clarity to focus on the effect of the push pulse.

accepted that the PB1 (~1.63 eV, 760 nm) and the PB2 (~2.58 eV, 480 nm) originate from the state filling of the band edge and dual valence and conduction bands, respectively (*11*, *13*).

We used PPP spectroscopy with a time resolution of <100 fs (Fig. 1A, inset) to investigate the higher excited state transition of the perovskite by probing the $+\Delta T$ [ground-state bleaching (GSB) and stimulated emission (SE)] signatures. The additional push pulse allows us to re-excite the equilibrated photoexcited state population to higher excited states and probe the transfer of HCs by monitoring the absence of thermalization signatures of the bleach. We carefully adjusted the radii of each beam such that $r_{pump} > r_{push} > r_{probe}$ (r_{pump} > 250 μm, 225 μm > r_{push} > 175 μm, and r_{probe} ~ 150 μm), to ensure uniform initial and secondary perturbation of the probed sample volume. In this work, a pump wavelength of 2.07 eV (600 nm) was used to generate the excited state carrier population, which was probed with a white-light continuum generated by a 2-mm-thick sapphire crystal. A push pulse arrives at t_{push} = 3 ps after initial photoexcitation and changes the transmittance of the probe pulse. In thin films where the reported thermalization times are less than 2 ps (*19*, *26*), delaying the push pulse to 3 ps allows the initial photogenerated carriers to sufficiently thermalize to the conduction band minimum (CBM) or valence band maximum (VBM). This allows the promotion of carriers from the same thermalized state to arbitrary higher excited states depending on the push wavelength. Since the push pulses can only partially repopulate the higher excited states, the excited carrier population is never fully depopulated (see Fig. 1B). As a result of the re-excitation, the higher excited state population can no longer be described by a Boltzmann or Fermi-Dirac distribution. Therefore, the push pulse re-excitation feature is leveraged to directly measure the higher excited states relaxation dynamics. Note that the push fluence is higher than what is normally used for the pump in TA as PPP is a nonlinear fifth-order process that involves an excited state absorption (ESA) (*27*) (i.e., about two orders of magnitude smaller than the linear absorption).

Figure 1C shows the pump-probe ("push off") and PPP ("push on") ΔT transients of MAPI. By taking the difference between the push off and push on ΔT signal, the corresponding PPP $\Delta\Delta T$ transients are obtained as illustrated in Fig. 1D. The samples are excited with 2.07 eV (600 nm) and pushed with 2.07 eV (600 nm) that is delayed by 3 ps, where the photoexcited carriers by then would have relaxed to the band edges. We selected a pump fluence of 5 μJ cm^{-2} because it falls within the linear range of the excitation (fig. S1). The probe is tuned to 1.63 eV (760 nm) to monitor the band-edge population. Although the 2.07-eV push pulse has a photon energy equivalent to the pump pulse, it hardly functions as a dump, where carriers in the excited state are forcibly relaxed by SE because the push has an energy higher than that of MAPI PL. Furthermore, secondary excitation from the ground state is also ruled out as the dominant process in our results (see figs. S2 and S3 and the Supplementary Materials for details). Expectedly, the 2.07-eV push pulse does function as a push (see figs. S4 and S5 for data and fits across the measurement window) because of the dominant PIA signature (Fig. 1A) arising from ESA and not because of the photoinduced change in the refractive index (see figs. S2 and S6) (*28*, *29*). After re-exciting a fraction of the band-edge population at 3 ps with the push pulse, the re-excited carrier population quickly cools back to the band edge on a subpicosecond time scale of ~0.4 ps, in agreement with the literature (*11*, *13*, *17*). Therefore, the sharp relaxation peak right after the push pulse indicates the HC thermalization back to the band-edge state. Note that, however, the original (before-push) band-edge population is not fully recovered, which indicates that some carriers are inadvertently lost in the process—possibly due to HC trapping and/or direct relaxation to the ground state via other recombination channels.

Interfacial energy barrier impeding HC extraction

We used bathophenanthroline (bphen) as the HC extractor, with highest occupied molecular orbital (HOMO) and lowest unoccupied molecular orbital (LUMO) offsets at ~1.0 and ~0.9 eV from perovskite VBM and CBM, respectively. The energy alignment of MAPI and bphen is illustrated in Fig. 1B (*30*, *31*). Such large energy difference makes it an ideal candidate for us to study the propensity of photoinduced HC extraction by using an additional push pulse to control the charge injection. The $\Delta\Delta T$ push-induced signal obtained for the MAPI/bphen sample (Fig. 2A, blue curve) reveals the interesting ultrafast behavior of the pushed carriers: The sharp push-induced peak (Fig. 2A, orange curve) completely vanishes. In MAPI/bphen,

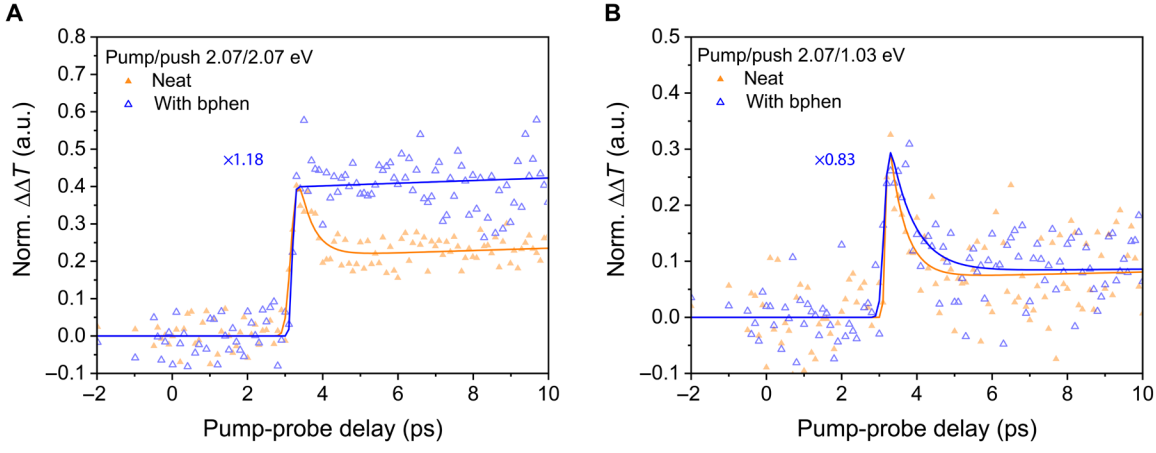

Fig. 2. Push-induced transients in MAPI. PPP $\Delta\Delta T$ push-induced signals of MAPI without (orange solid symbols) and with bphen (blue open symbols) quenching layer probed at PB1 obtained by taking the push-on and push-off difference from the ΔT transients. The push pulse arrives 3 ps after the 2.07-eV pump (5 μJ cm^{-2}), with varying energies to probe different excited states; (**A**) 2.07 eV (15 μJ cm^{-2}) and (**B**) 1.03 eV (650 μJ cm^{-2}). Solid lines are exponential fits of the pump-probe ΔT signals, and the raw data are depicted by symbols. For clarity, the transients of MAPI with bphen are scaled by a factor of 1.18 in (A) and 0.83 in (B).

the HCs that are promoted to higher excited states by the 2.07-eV push (using a fluence of 15 μJ cm^{-2}) will have sufficient energy to be injected into bphen. Thus, accounting for the disappearance of the fast decay (i.e., absence of the ultrafast carrier cooling transient back to the band edge), the HCs, now in bphen, will not be able to relax back to the MAPI conduction band edge.

Although a 2.07-eV push measurement on MAPI/bphen is adequate proof of HC extraction, there is a lower limit of push photon energies needed to realize this. Figure 2B shows the push pulse with 1.03 eV (using a fluence of 650 μJ cm^{-2}) that is still higher than the bphen acceptor level. For the neat MAPI film in the absence of bphen (orange curves), the familiar fast decay on the subpicosecond time scale in the push-induced signal is observed for all push photon energies. As before, this process is directly attributed to cooling of the pushed excited carrier population back to the CBM (i.e., recovery of band-edge population). However, the sharp peak remains virtually unchanged in the MAPI/bphen samples at 1.03-eV push energy. This indicates that there is a threshold energy needed to overcome the potential barrier between MAPI and bphen to initiate carrier extraction.

To determine the interface barrier more accurately, we performed PPP measurements with fine-tuning of the push pulse energies (Fig. 3A). The step-like PPP transients (indicating efficient HC extraction) at 2.07 and 1.98 eV (10 μJ cm^{-2}) push change into small peak-shaped transients (some HC extraction) at 1.91 and 1.77 eV (10 μJ cm^{-2}), with the sharp peaks developed at 1.03 eV (very poor/no HC extraction). From this, we estimate that the barrier height is between 1.01 and 1.08 eV above the LUMO energy level of bphen for complete transfer of HCs. A consequence of this barrier and the large energy difference between the acceptor levels of bphen and the CBM and VBM of MAPI is seen in Fig. 3B, where the direct photogenerated carriers, singly pumped with a 3.10-eV pulse (using a fluence of 5 μJ cm^{-2} fluence), are not extracted by bphen (absence of quenching). The results confirm that, at minimum, a 1.98-eV push photon is sufficiently energetic to allow HCs to completely transfer or tunnel from MAPI to bphen. We ascribe this to an interfacial Schottky barrier that forms when the two materials are in contact. It is not possible to carry out direct excitation of MAPI (pump at 3.5 eV to overcome the barrier) and monitor the ground-state bleach signal in bphen to observe the charge transfer because a 3.5-eV photon would also generate excited carrier populations in bphen. Pump-probe spectroscopy would not be able to resolve whether the signal comes from the photogenerated carriers in bphen or due to charge transfer of carriers from MAPI to bphen.

DISCUSSION

Last, we would like to emphasize the subtle differences between interpreting HC dynamics in TA and PPP spectroscopy, particularly on the comparison of the fluence used and the carrier temperatures of the HCs. The common approach of TA data analysis to extract carrier cooling times involves tracking the time-dependent carrier temperature, obtained by fitting the high-energy tail with a Boltzmann distribution from 0.3 ps and later (*13*, *14*, *17*). Theoretically, this method could provide the HC cooling time, which is the time for the HC distribution to thermally equilibrate with the lattice, but the data analysis is not as straightforward in practice. A high-fluence pump creates a large population of HCs that gives rise to carrier density–dependent effects. These include hot phonon bottlenecks, Burstein-Moss, and bandgap renormalization that can influence the spectral features and the high-energy tail. The latter two effects affect the perovskite's bandgap, causing a blue shift and red shift, respectively.

In the case of TA spectroscopy, the HC population at thermal equilibrium can be described by the Boltzmann distribution. Assuming a thermalized HC temperature of T_c ~ 1000 K in bulk perovskite films (*14*), the Boltzmann equation is used to estimate that only a fraction of the population above k_BT_c (~37%), at a level ~86 meV above the band edge, can be extracted as HCs, as illustrated in Fig. 4. The large fraction of the remaining HC population (~63%) would still be distributed in energetically confined states below k_BT_c ~86 meV. In sharp contrast, for PPP spectroscopy, the ability to repopulate specific higher excited states enables us to directly probe the intrinsic lifetimes of these states that are free from multiband excitation and density-dependent multiparticle effects. In our measurements, we estimate that approximately 30 to 40% of the initial photoexcited

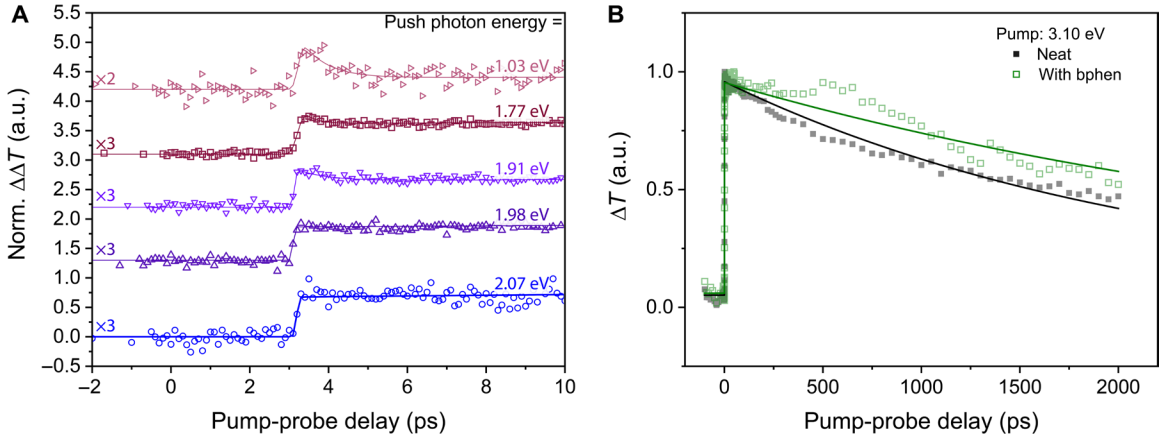

Fig. 3. Determining the interface barrier in MAPI/bphen. (**A**) Push photon energy–dependent ΔΔ*T* measurements at finer intervals, 2.07 eV (blue circles, 15 μJ cm^{-2}), 1.98 eV (dark purple upright triangles, 10 μJ cm^{-2}), 1.91 eV (purple inverted triangles, 10 μJ cm^{-2}), 1.77 eV (maroon squares, 10 μJ cm^{-2}), and 1.03 eV (pink right triangles, 650 μJ cm^{-2}) reveal that, at minimum, a 1.98-eV push photon is required to overcome the barrier between MAPI and bphen. The transients are scaled according to the factors denoted in the graph and offset for clear comparison. (**B**) Transient transmission dynamics of MAPI pumped at 3.10 eV (400 nm, 5 μJ cm^{-2}) and probed at 1.63 eV (760 nm) reveals no quenching of the lifetime. This indicates that the photoexcited carriers are not able to be extracted by bphen. Slight lengthening of the lifetime comes from surface trap passivation by the bphen layer.

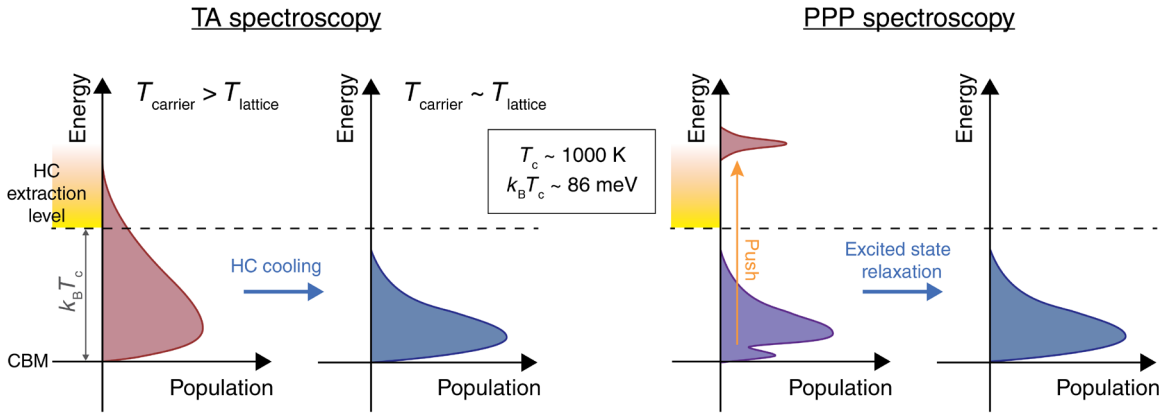

Fig. 4. Schematic comparison of the carrier population under probe. In TA spectroscopy, at thermalized carrier temperatures of $T_c \sim 1000$ K, i.e., ~ 86 meV above the band edge, only a fraction (37%) exists. This contrasts with PPP spectroscopy, where a fraction of the excited carrier population is re-excited above the LUMO level of the HC acceptor, and the excited state lifetime is directly probed. Here, we assume a pump wavelength of 400 nm and an excited carrier density of 10^{18} cm^{-3}.

carrier population is re-excited. Hence, the relatively lower excited carrier population minimizes the influence of such multiparticle effects and allows us to clearly probe the intrinsic HC dynamics. Nonetheless, it is the collective behavior of the HCs (i.e., density-dependent multiparticle effects, phonon bottleneck, etc.) under continuous solar flux that determines the operation in practical HC solar cells.

In summary, we explicate the intrinsic photophysics of the higher excited states in MAPI by re-exciting a fraction of carriers to higher-energy levels using PPP spectroscopy. This allows us to circumvent complications arising from multiparticle effects commonly seen in TA spectroscopy. The HCs can be extracted using a narrow electron bandwidth semiconducting molecular bphen electron acceptor in thin-film geometry. This extraction is substantiated by the absence of the ultrafast subpicosecond decay from the PPP $\Delta\Delta T$ transients, indicating that the transfer times are much faster than the sub-picosecond cooling times. The extraction is, however, impeded by an interfacial barrier formed between MAPI and bphen, which imposes a threshold push energy. Given that MAPI absorbs over a broad solar spectrum, both HCs and "cold carriers" (near the band edge) are simultaneously created. Presently, extraction of HCs without sacrificing the cold carriers is an open question in the device architecture of HC solar cells, which underscores the complexities of realizing practical HC perovskite solar cells. Our findings pave the way for exploring such acceptors as selective energy contacts for practical HC perovskite solar cells to surpass the fundamental detailed balance limit of perovskite solar cells and in the context of concentrated photovoltaic systems.

MATERIALS AND METHODS

Thin-film preparation

The single-step 12.5% stoichiometric solution was prepared in an N2-filled glove box by mixing equal molar of methylammonium iodide (CH_3NH_3I) (Dyesol) and PbI_2 (99%; Acros Organics) in anhydrous *N*,*N*-dimethylforamide (99.9%; Sigma-Aldrich) and stirred at 70°C for 2 hours. The solution was further stirred for 30 min and filtered with a 0.45-μm polytetrafluoroethylene filter before spin coating. The perovskite solution was spin-coated on quartz substrates at 5000 rpm for 12 s. Solvent engineering was performed by dripping 100 μl of toluene 3 s into the start of the spin coating, and the samples were then annealed at 100°C for 30 min. A 100-nm-thick bphen (97%; Sigma-Aldrich) was then evaporated at a rate of 0.2 to 0.3 Å s^{-1} for the first 20 nm and 0.3 to 0.5 Å s^{-1} for the remaining 80 nm at ~8×10^{-4} Pa.

PPP spectroscopy

Femtosecond PPP experiments were performed with a home-built setup in transmission geometry. A small portion of the output from a Coherent Libra regenerative amplifier (50 fs, 1 kHz, 800 nm) was split off to generate a white-light continuum, while the remainder was used to pump two Coherent OPerA Solo optical parametric amplifiers (OPAs). A 750-nm short-pass filter was placed in the probe arm before the sample to attenuate the 800-nm fundamental beam used for white-light continuum generation (we estimated a probe fluence of ~0.14 μJ cm^{-2} at ~1.63 eV). One OPA was used to generate the pump pulse train (2.07 or 3.10 eV), and the other OPA was used to generate the push pulse train. The pump is chopped at 83 Hz, in combination with a modulated push, and the pump-probe and PPP signals can be obtained separately and averaged across at least three scans. Taking the difference yields the push-induced signal (described in the main text under the section "Carrier relaxation probed by PPP spectroscopy"). Both push and probe pulse trains are mechanically delayed by precision delay stages, and the probe is collected by a spectrometer (Princeton Instruments Acton SP-2300i) coupled to a photomultiplier tube point detector and collected by the computer through an SRS 830 lock-in amplifier.

SUPPLEMENTARY MATERIALS

Supplementary material for this article is available at http://advances.sciencemag.org/cgi/content/full/5/11/eaax3620/DC1

Section S1. Interpretation of PPP signal
Section S2. Charge extraction to bphen
Section S3. PIA modeling based on refractive index change
Fig. S1. Pump fluence–dependent measurements.
Fig. S2. Push-induced photophysical processes.
Fig. S3. Push-induced transient transmission dynamics of MAPI.
Fig. S4. Push-induced transients in MAPI.
Fig. S5. Comparison of fitting models.
Fig. S6. Complex refractive index of MAPI.
Table S1. *F* test parameter report.

Table S2. *F* test analysis.
Table S3. List of parameters.
References (*32*–*35*)

REFERENCES AND NOTES

1. NREL (National Renewable Energy Laboratory), Photovoltaic research: Best research-cell efficiency chart. (2019). https://www.nrel.gov/pv/cell-efficiency.html.
2. H. Cho, S.-H. Jeong, M.-H. Park, Y. H. Kim, C. Wolf, C.-L. Lee, J. H. Heo, A. Sadhanala, N. Myoung, S. Yoo, S. H. Im, R. H. Friend, T.-W. Lee, Overcoming the electroluminescence efficiency limitations of perovskite light-emitting diodes. *Science* **350**, 1222–1225 (2015).
3. G. Li, Z.-K. Tan, D. Di, M. L. Lai, L. Jiang, J. H.-W. Lim, R. H. Friend, N. C. Greenham, Efficient light-emitting diodes based on nanocrystalline perovskite in a dielectric polymer matrix. *Nano Lett.* **15**, 2640–2644 (2015).
4. G. Xing, N. Mathews, S. S. Lim, N. Yantara, X. Liu, D. Sabba, M. Grätzel, S. Mhaisalkar, T. C. Sum, Low-temperature solution-processed wavelength-tunable perovskites for lasing. *Nat. Mater.* **13**, 476–480 (2014).
5. F. Deschler, M. Price, S. Pathak, L. E. Klintberg, D. D. Jarausch, R. Higler, S. Hüttner, T. Leijtens, S. D. Stranks, H. J. Snaith, M. Atatüre, R. T. Phillips, R. H. Friend, High photoluminescence efficiency and optically-pumped lasing in solution-processed mixed halide perovskite semiconductors. *J. Phys. Chem. Lett.* **5**, 1421–1426 (2014).
6. W. Shockley, H. J. Queisser, Detailed balance limit of efficiency of *p-n* junction solar cells. *J. Appl. Phys.* **32**, 510–519 (1961).
7. J. M. Richter, F. Branchi, F. Valduga de Almeida Camargo, B. Zhao, R. H. Friend, G. Cerullo, F. Deschler, Ultrafast carrier thermalization in lead iodide perovskite probed with two-dimensional electronic spectroscopy. *Nat. Commun.* **8**, 376 (2017).
8. J. Shah, *Ultrafast Spectroscopy of Semiconductors and Semiconductor Nanostructures* (Springer Berlin Heidelberg, 1996), vol. 115.
9. M. A. Green, G. Conibeer, D. König, S. Shrestha, S. Huang, P. Aliberti, L. Treiber, R. Patterson, B. P. Veettil, A. Hsieh, Y. Feng, A. Luque, A. Marti, P. G. Linares, E. Canovas, E. Antolin, D Fuertes Marrón, C. Tablero, E. Hernandez, J. F. Guillemoles, L. Huang, A Le Bris, T. Schmidt, R. Clady, M. Tayebjee, Hot carrier solar cells: Challenges and recent progress, in *2010 35th IEEE Photovoltaic Specialists Conference* (IEEE, 2010), pp. 000057–000060.
10. R. T. Ross, A. J. Nozik, Efficiency of hot-carrier solar energy converters. *J. Appl. Phys.* **53**, 3813–3818 (1982).
11. G. Xing, N. Mathews, S. Sun, S. S. Lim, Y. M. Lam, M. Grätzel, S. Mhaisalkar, T. C. Sum, Long-range balanced electron- and hole-transport lengths in organic-inorganic $CH_3NH_3PbI_3$. *Science* **342**, 344–347 (2013).
12. T. C. Sum, N. Mathews, G. Xing, S. S. Lim, W. K. Chong, D. Giovanni, H. A. Dewi, Spectral features and charge dynamics of lead halide perovskites: Origins and interpretations. *Acc. Chem. Res.* **49**, 294–302 (2016).
13. Y. Yang, D. P. Ostrowski, R. M. France, K. Zhu, J. van de Lagemaat, J. M. Luther, M. C. Beard, Observation of a hot-phonon bottleneck in lead-iodide perovskites. *Nat. Photonics* **10**, 53–59 (2016).
14. J. Fu, Q. Xu, G. Han, B. Wu, C. H. A. Huan, M. L. Leek, T. C. Sum, Hot carrier cooling mechanisms in halide perovskites. *Nat. Commun.* **8**, 1300 (2017).
15. H.-H. Fang, S. Adjokatse, S. Shao, J. Even, M. A. Loi, Long-lived hot-carrier light emission and large blue shift in formamidinium tin triiodide perovskites. *Nat. Commun.* **9**, 243 (2018).
16. H. Zhu, K. Miyata, Y. Fu, J. Wang, P. P. Joshi, D. Niesner, K. W. Williams, S. Jin, X.-Y. Zhu, Screening in crystalline liquids protects energetic carriers in hybrid perovskites. *Science* **353**, 1409–1413 (2016).
17. M. B. Price, J. Butkus, T. C. Jellicoe, A. Sadhanala, A. Briane, J. E. Halpert, K. Broch, J. M. Hodgkiss, R. H. Friend, F. Deschler, Hot-carrier cooling and photoinduced refractive index changes in organic-inorganic lead halide perovskites. *Nat. Commun.* **6**, 8420 (2015).
18. Y. Yang, M. Yang, Z. Li, R. Crisp, K. Zhu, M. C. Beard, Comparison of recombination dynamics in $CH_3NH_3PbBr_3$ and $CH_3NH_3PbI_3$ perovskite films: Influence of exciton binding energy. *J. Phys. Chem. Lett.* **6**, 4688–4692 (2015).
19. M. Li, S. Bhaumik, T. W. Goh, M. S. Kumar, N. Yantara, M. Grätzel, S. Mhaisalkar, N. Mathews, T. C. Sum, Slow cooling and highly efficient extraction of hot carriers in colloidal perovskite nanocrystals. *Nat. Commun.* **8**, 14350 (2017).
20. Z. Guo, Y. Wan, M. Yang, J. Snaider, K. Zhu, L. Huang, Long-range hot-carrier transport in hybrid perovskites visualized by ultrafast microscopy. *Science* **356**, 59–62 (2017).
21. M. Li, R. Begum, J. Fu, Q. Xu, T. M. Koh, S. A. Veldhuis, M. Grätzel, N. Mathews, S. Mhaisalkar, T. C. Sum, Low threshold and efficient multiple exciton generation in halide perovskite nanocrystals. *Nat. Commun.* **9**, 4197 (2018).
22. M. S. Marek, T. Buckup, J. Southall, R. J. Cogdell, M. Motzkus, Highlighting short-lived excited electronic states with pump-degenerate-four-wave-mixing. *J. Chem. Phys.* **139**, 074202 (2013).
23. A. A. Bakulin, A. Rao, V. G. Pavelyev, P. H. M. van Loosdrecht, M. S. Pshenichnikov, D. Niedzialek, J. Cornil, D. Beljonne, R. H. Friend, The role of driving energy and delocalized states for charge separation in organic semiconductors. *Science* **335**, 1340–1344 (2012).
24. C. Gadermaier, G. Cerullo, G. Sansone, G. Leising, U. Scherf, G. Lanzani, Time-resolved charge carrier generation from higher lying excited states in conjugated polymers. *Phys. Rev. Lett.* **89**, 117402 (2002).
25. P. C. Tapping, T. W. Kee, Optical pumping of poly(3-hexylthiophene) singlet excitons induces charge carrier generation. *J. Phys. Chem. Lett.* **5**, 1040–1047 (2014).
26. T. R. Hopper, A. Gorodetsky, J. M. Frost, C. Müller, R. Lovrincic, A. A. Bakulin, Ultrafast intraband spectroscopy of hot-carrier cooling in lead-halide perovskites. *ACS Energy Lett.* **3**, 2199–2205 (2018).
27. G. M. Paternò, L. Moretti, A. J. Barker, Q. Chen, K. Müllen, A. Narita, G. Cerullo, F. Scotognella, G. Lanzani, Pump–push–probe for ultrafast all-optical switching: The case of a nanographene molecule. *Adv. Funct. Mater.* **29**, 1805249 (2018).
28. T. Ghosh, S. Aharon, A. Shpatz, L. Etgar, S. Ruhman, Reflectivity effects on pump–probe spectra of lead halide perovskites: Comparing thin films versus nanocrystals. *ACS Nano* **12**, 5719–5725 (2018).
29. R. R. Tamming, J. Butkus, M. B. Price, P. Vashishtha, S. K. K. Prasad, J. E. Halpert, K. Chen, J. M. Hodgkiss, Ultrafast spectrally resolved photoinduced complex refractive index changes in $CsPbBr_3$ perovskites. *ACS Photonics* **6**, 345–350 (2019).
30. F. Hou, Z. Su, F. Jin, X. Yan, L. Wang, H. Zhao, J. Zhu, B. Chu, W. Li, Efficient and stable planar heterojunction perovskite solar cells with an MoO_3/PEDOT:PSS hole transporting layer. *Nanoscale* **7**, 9427–9432 (2015).
31. H. Yang, S. Cong, Y. Lou, L. Han, J. Zhao, Y. Sun, G. Zou, Organic–inorganic hybrid interfacial layer for high-performance planar perovskite solar cells. *ACS Appl. Mater. Interfaces* **9**, 31746–31751 (2017).
32. T. W. Kee, Femtosecond pump–push–probe and pump–dump–probe spectroscopy of conjugated polymers: New insight and opportunities. *J. Phys. Chem. Lett.* **5**, 3231–3240 (2014).
33. W. Kong, T. Ding, G. Bi, H. Wu, Optical characterizations of the surface states in hybrid lead–halide perovskites. *Phys. Chem. Chem. Phys.* **18**, 12626–12632 (2016).
34. M. Saba, M. Cadelano, D. Marongiu, F. Chen, V. Sarritzu, N. Sestu, C. Figus, M. Aresti, R. Piras, A. Geddo Lehmann, C. Cannas, A. Musinu, F. Quochi, A. Mura, G. Bongiovanni, Correlated electron–hole plasma in organometal perovskites. *Nat. Commun.* **5**, 5049 (2014).
35. Q. Lin, A. Armin, R. C. R. Nagiri, P. L. Burn, P. Meredith, Electro-optics of perovskite solar cells. *Nat. Photonics* **9**, 106–112 (2015).

Acknowledgments: We thank S. Ruhman for discussions on the photoinduced absorption signatures. We thank M. Righetto for discussions on the statistical tests. **Funding:** Financial support from the Nanyang Technological University start-up grant M4080514, the JSPS-NTU Joint Research Project M4082176, the Ministry of Education AcRF Tier 1 grant RG173/16 and Tier 2 grants MOE2015-T2-2-015, MOE2016-T2-1-034, and MOE2017-T2-2-002, the U.S. Office of Naval Research (ONRGNICOPN62909-17-1-2155), and the Singapore National Research Foundation (Programs NRF-CRP14-2014-03, NRF2018-ITC001-001, and NRF-NRFI-2018-04) is acknowledged. **Author contributions:** T.C.S., S.S.L., and D.G. conceived the idea and designed the experiments. S.S.L. and D.G. performed the spectroscopic characterization. J.W.M.L. performed the fluence-dependent measurement. Q.Z., A.S., N.F.J., N.M., and S.M. prepared the samples. S.S.L., D.G., M.S.P., and T.C.S. analyzed the data and wrote the manuscript. All authors discussed the results and commented on the manuscript at all stages. T.C.S. led the project. This work was done as part of S.S.L.'s Ph.D. thesis entitled "Engineering Carrier Dynamics in Lead Halide Perovskites." **Competing interests:** The authors declare that they have no competing interests. **Data and materials availability:** All data needed to evaluate the conclusions in the paper are present in the paper and/or the Supplementary Materials. The data will be uploaded to DR-NTU, an institutional data repository, and can be accessed via https://doi.org/10.21979/N9/RZUNHG. Additional data related to this paper may be requested from the authors.

Submitted 18 March 2019
Accepted 18 September 2019
Published 15 November 2019
10.1126/sciadv.aax3620

Citation: S. S. Lim, D. Giovanni, Q. Zhang, A. Solanki, N. F. Jamaludin, J. W. M. Lim, N. Mathews, S. Mhaisalkar, M. S. Pshenichnikov, T. C. Sum, Hot carrier extraction in $CH_3NH_3PbI_3$ unveiled by pump-push-probe spectroscopy. *Sci. Adv.* **5**, eaax3620 (2019).

Science Advances

Hot carrier extraction in $CH_3NH_3PbI_3$ unveiled by pump-push-probe spectroscopy

Swee Sien Lim, David Giovanni, Qiannan Zhang, Ankur Solanki, Nur Fadilah Jamaludin, Jia Wei Melvin Lim, Nripan Mathews, Subodh Mhaisalkar, Maxim S. Pshenichnikov and Tze Chien Sum

Sci Adv **5** (11), eaax3620.
DOI: 10.1126/sciadv.aax3620